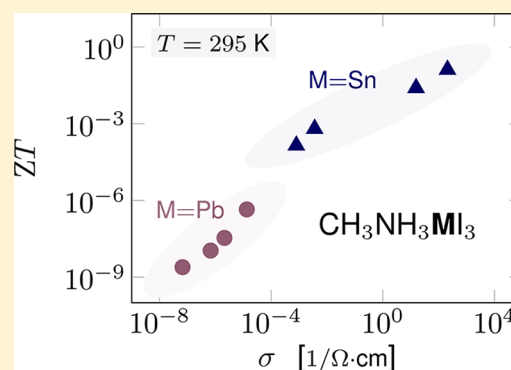


Tuning of the Thermoelectric Figure of Merit of $\text{CH}_3\text{NH}_3\text{MI}_3$ ($\text{M}=\text{Pb},\text{Sn}$) Photovoltaic Perovskites

Xavier Mettan,* Riccardo Pisoni, Péter Matus, Andrea Pisoni, Jaćim Jaćimović, Bálint Náfrádi, Massimo Spina, Davor Pavuna, László Forró, and Endre Horváth

Laboratory of Physics of Complex Matter, EPFL, CH-1015 Lausanne, Switzerland

ABSTRACT: The hybrid halide perovskites, the very performant compounds in photovoltaic applications, possess large Seebeck coefficient and low thermal conductivity, making them potentially interesting high figure of merit (ZT) materials. For this purpose, one needs to tune the electrical conductivity of these semiconductors to higher values. We have studied the $\text{CH}_3\text{NH}_3\text{MI}_3$ ($\text{M}=\text{Pb},\text{Sn}$) samples in pristine form showing very low ZT values for both materials; however, photoinduced doping (in $\text{M}=\text{Pb}$) and chemical doping (in $\text{M}=\text{Sn}$) indicate that, by further doping optimization, ZT can be enhanced toward unity and reach the performance level of the presently most efficient thermoelectric materials.



I. INTRODUCTION

Thermoelectric materials have great potential for future device applications in energy conversion because they transform a temperature gradient, imposed across their volume, into electricity.^{1,2} They are especially foreseen to harvest electrical current from waste-heat production.³ Solar thermoelectric generation is an emerging technology combining concentrated solar power and thermoelectric effect.⁴ Here the solar light is collected to generate the temperature gradient across the active thermoelectric material. The success of this technique strongly relies on the efficiency of the thermoelectric materials involved. The efficiency of thermoelectric devices is determined by a dimensionless parameter called figure of merit (ZT), which corresponds to the energy conversion efficiency of a Carnot cycle.¹ ZT is defined as $(S^2\sigma/\kappa)T$, where T is the absolute temperature, S is the Seebeck coefficient (or thermoelectric power), σ is the electrical conductivity, and κ is the thermal conductivity. The best known thermoelectric materials have a ZT in the range of 2.⁵ Nevertheless, synthesizing materials with a higher ZT would be highly beneficial. Therefore, there is a constant search for engineering thermoelectric materials with a high AT , in addition to low production costs. Lately, hybrid halide perovskites $\text{CH}_3\text{NH}_3\text{PbI}_3$ (hereafter MAPbI_3) and $\text{CH}_3\text{NH}_3\text{SnI}_3$ (hereafter MASnI_3) have been considered for thermoelectric applications because they possess an extremely large Seebeck coefficient and an unusually low thermal conductivity.⁶ Theoretical modeling of He and Galli⁷ have foreseen that with suitable doping the ZT value of these two compounds could raise into the range required for thermoelectric applications. In this work, we systematically investigate the transport properties and the figure of merit of potentially low-cost and solution-processable MAPbI_3 and MASnI_3

samples, studying their evolution with photo and impurity doping.

II. EXPERIMENTAL SECTION

MAPbI₃ and MASnI₃ Synthesis. Single crystals of MAPbI_3 and MASnI_3 were prepared by solution growth. MAPbI_3 single crystals were prepared by precipitation from a concentrated aqueous solution of hydriodic acid (57 wt % in H_2O , 99.99% Sigma-Aldrich) containing lead(II) acetate trihydrate (99.999%, Acros Organics) and a respective amount of CH_3NH_2 solution (40 wt % in H_2O , Sigma-Aldrich). A constant 55–42 °C temperature gradient was applied to induce saturation of the solute in the low temperature region of the solution. After 24 h, submillimeter-sized flake-like nuclei were floating on the surface of the solution (see supporting information of ref 8). Large cube-like and rhombohedral MAPbI_3 crystals with 3–5 mm silver-gray facets were obtained after 7 days (left inset of Figure 1). MASnI_3 crystals were prepared by precipitation from a concentrated aqueous solution of hydriodic acid (57 wt % in H_2O , 99.99% Sigma-Aldrich) containing tin(IV) iodide and a respective amount of CH_3NH_2 solution (40 wt % in H_2O , Sigma-Aldrich). Tin(IV) iodide was previously prepared by the reaction of tin(II) chloride (99.99% Sigma-Aldrich) and a respective amount of hydriodic acid (57 wt % in H_2O , 99.99% Sigma-Aldrich). The bright orange solid was subsequently filtered and dried at 80 °C. Usually MASnI_3 crystals are of smaller size and very often heavily twinned (right inset of Figure 1). To prevent any unwanted reaction of the samples with moisture and air, the as-synthesized crystals were

Received: April 24, 2015

Revised: May 1, 2015

Published: May 3, 2015

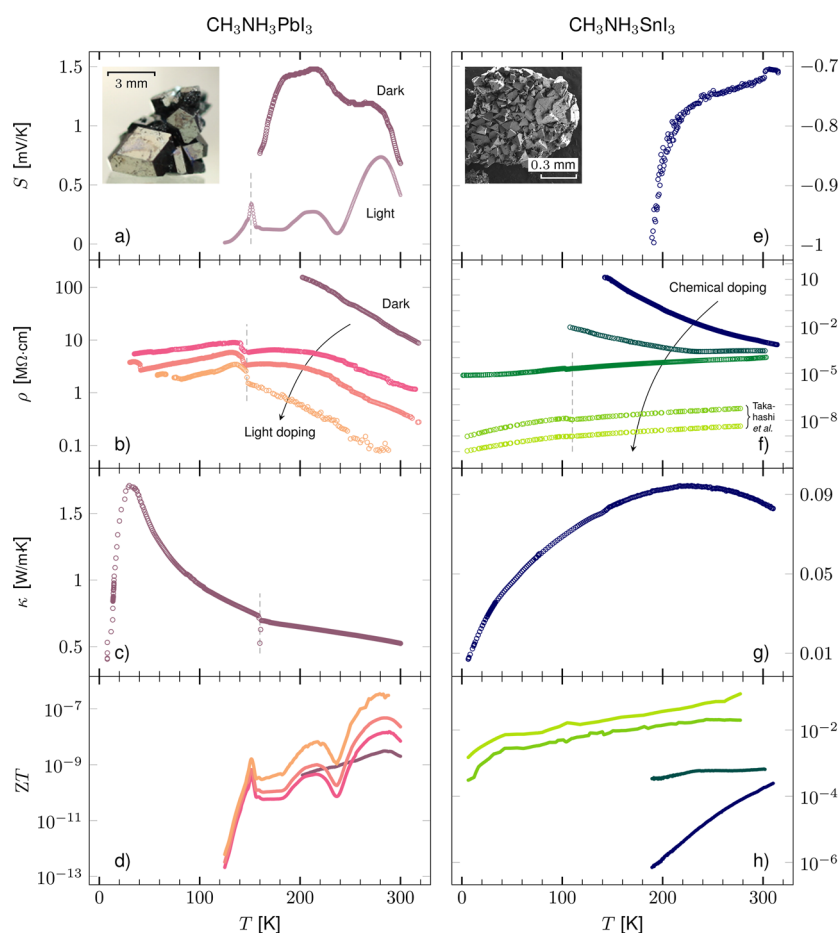


Figure 1. From top to bottom: thermoelectric power, S , electrical resistivity, ρ , thermal conductivity, κ , and figure of merit, ZT , of $\text{CH}_3\text{NH}_3\text{PbI}_3$ (left panel) and $\text{CH}_3\text{NH}_3\text{SnI}_3$ (right panel) for light (photoelectron) and impurity doping. The three curves of MAPbI_3 , red, orange, and yellow correspond to light intensities of 80, 165, and 220 mW/cm^2 . κ of MAPbI_3 (c) was reproduced from ref 6, and the two lowermost $\rho(T)$ of MASnI_3 (f) were reproduced from ref 10. The vertical dashed lines denote a structural phase transition observed in both MAPbI_3 and MASnI_3 . Left inset: Optical image of a MAPbI_3 crystal. Right inset: Scanning electron microscope image of a MASnI_3 crystallite.

immediately transferred and kept in a desiccator prior to the measurements. Because we observed a possible dependency of S , ρ , and $\kappa(T)$ on the environmental conditions, every measurement was performed under high vacuum ($p \leq 5 \times 10^{-5}$ mbar). In this way, possible undesirable ionic conduction induced by water as well as thermal dissipation in the surrounding gas were avoided. The MASnI_3 crystallites were compressed into pellets to allow a more reliable measurement of the transport coefficients, while the MAPbI_3 crystals were directly connected for transport measurements.

Electrical and Thermal Transports Characterization. A conventional four-point technique was employed to measure the resistivity. Gold wires were glued on the sample with carbon-containing paste to minimize the Schottky barrier at the interface. For the measurement of the Seebeck coefficient, a temperature gradient was imposed by a resistive heater attached to one extremity of the sample, driven by an alternating current of frequency $f = 60$ mHz. The temperature gradient across the sample was measured by a Chromel–Constantan (Type E) differential thermocouple, using a lock-in amplifier at $2f$. The temperature gradient was carefully set to be smaller than 1 K. The thermoelectric voltage was amplified by a Keithley 6517 electrometer and determined using a lock-in amplifier at $2f$. This measurement was performed on polycrystalline samples as well, without noticeable difference with the values obtained on

single crystals. The thermal conductivity of MASnI_3 was measured in a configuration previously described elsewhere,^{6,9} whereas for MAPbI_3 , data are recovered from a previous publication of our group.⁶ κ was measured by a steady-state method, using calibrated stainless steel as reference sample. The temperature gradient across the sample was kept around 1 K, and it was measured with type E differential thermocouples connected to the sample and the reference with Stycast 2859 Ft thermal conducting epoxy. The electrical resistivity of the same MAPbI_3 crystal was measured in the dark and under white-light illumination of 80, 165, and 220 mW/cm^2 (in Figures 1 and 2: red, orange, and yellow curves, respectively). Measurements of the Seebeck coefficient were performed on the same sample in dark and under white-light emanating from a light-emitting diode (LED). MASnI_3 crystals from different syntheses were employed for measurements of ρ . The Seebeck coefficient of MASnI_3 was measured for the most resistive sample. No light intensity dependency was observed in the ρ and S values for MASnI_3 ; therefore, all of the measurements were conducted in dark. The thermal conductivity of MASnI_3 was measured on the same sample as the one studied for Seebeck coefficient. We investigated a temperature range from 4 to 300 K, for every measurement of S , ρ , and κ ; however, because of the high resistance of some of the samples, we were often limited to narrower temperature ranges (e.g., for S of MAPbI_3 and

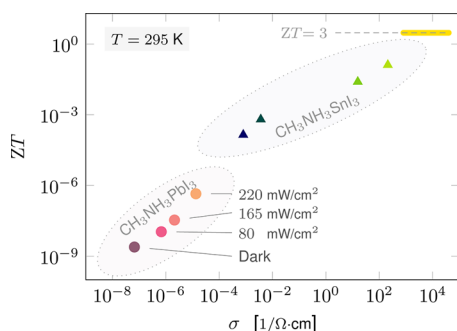


Figure 2. Summary of the evolution of the figure of merit ZT at room temperature ($T = 295$ K), with doping monitored through the conductivity increase with photo and impurity doping. The color map matches the one in Figure 1. The dashed line marks $ZT = 3$, a value attractive for applications. This requires a resistivity in the 1×10^{-3} to $3 \times 10^{-5} \Omega \text{ cm}$ range (yellow colored zone), accessible by appropriate doping.

MASnI₃ and for ρ of MAPbI₃ in dark and of MASnI₃ at low doping levels).

III. RESULTS AND DISCUSSION

The temperature-dependent transport coefficients S , ρ , κ , and the resulting ZT are reported for both MAPbI₃ and MASnI₃ in Figure 1. The resistivity and thermoelectric power of MASnI₃ have already been explored recently,^{10–12} whereas the resistivity and thermal conductivity of MAPbI₃ in dark have been discussed in ref 6. The resistivity of MAPbI₃ (Figure 1b) in the dark is smoothly decreasing with increasing temperatures ($d\rho/dT < 0$), reaching $\rho(295 \text{ K}) = 15 \text{ M}\Omega \text{ cm}$. Upon white-light illumination the resistivity globally decreases up to more than two orders of magnitude as an increasing number of photoexcited carriers become available for conduction. When the intensity of white light increases, the absolute value of ρ decreases. The kink at 150 K accounts for the structural phase transition from a tetragonal to an orthorhombic symmetry of the lattice. Furthermore, the effect of the phase transition can also be seen in the thermoelectric power (Figure 1a) and thermal conductivity temperature dependencies (Figure 1c). The observed small shift in the temperature of this transition might be due to some heating effect of the lamp. At $T < 150$ K, ρ of the illuminated sample decreases with lowering temperature in a metal-like behavior. This unexpected behavior will be addressed in more detail in a forthcoming work (unpublished results).

The temperature dependency of the Seebeck coefficient of MAPbI₃ follows a nontrivial behavior with peaks appearing at $T \approx 270$, 215, and 190 K in the dark and at ≈ 280 and 210 K under white-light illumination. The absolute value of the thermoelectric power of MAPbI₃ was found to be slightly sample-dependent; however, the overall temperature behavior is similar from one sample to another. The positive Seebeck coefficient argues for holes as the dominant type of charge carriers, but its nonmonotonic temperature dependency indicates that electrons, whose temperature-dependent mobility differs from the one of holes, also participate in the charge transport. Independent variations of the contributions of holes (or electrons) weighted by their respective mobilities to the Seebeck coefficient could be the reason for some of the peaks. The decrease in S at room temperature (295 K) upon illumination, from $S_{\text{dark}} = 0.82 \text{ mV/K}$ to $S_{\text{light}} = 0.54 \text{ mV/K}$, is

consistent with the resistivity data because electrons are photoinduced in the conduction band, decreasing the absolute value of S .

The temperature-dependent resistivity of MASnI₃ samples (Figure 1f) varies from a thermally activated behavior (with activation energy E_a equal to 0.25 eV) to a metallic one for the different samples investigated. It has been previously reported that MASnI₃ is a doped semiconductor.¹² The presence of an unknown but significant amount of impurity levels within the MASnI₃ band gap is at the origin of this varying $\rho(T)$. The material has been intentionally doped by Takahashi et al.,¹⁰ thus allowing to obtain a metallic behavior. Two of their $\rho(T)$ curves are reprinted there (Figure 1f). The observed tunability of the electrical conductivity in MASnI₃ is therefore expected to be like in other extrinsic semiconductors.¹³ Thus, by doping MASnI₃, it is possible to obtain larger carrier densities and optimize the thermoelectric properties.

The negative sign of S of MASnI₃ (Figure 1e) indicates that the majority carriers are electrons, in agreement with a previous study;¹⁴ however, the negative sign is in contradiction with some previous results.¹⁰ This discrepancy might be due to the different nature of the impurity levels present in the band gap. A predominant number of donor over acceptor impurity levels explains the negative sign observed in our sample. The absolute value of $S(295 \text{ K}) = -0.72 \text{ mV/K}$ is rather high, one order of magnitude larger than the value reported in ref 14, because the samples under consideration are semiconducting. Upon doping, S decreases (not shown), and for the metallic samples, it has a linear temperature dependency.¹⁰ Its value stays in the 100 $\mu\text{V/K}$ range at 295 K.

The thermal conductivity of both compounds is very low, presumably because of the rattling motion of the organic cation, but for MASnI₃, $\kappa = 0.09 \pm 0.01 \text{ W/m K}$ is even lower than the one observed in MAPbI₃ ($\kappa = 0.5 \pm 0.1 \text{ W/m K}$)⁶ (Figure 1g). This could be partially due to the polycrystalline nature of the MASnI₃ sample studied; however, the overall temperature dependency of κ in MASnI₃ is very different from the one in MAPbI₃. The broad maximum around 220 K suggests that there are some small structural motives that limit the phonon mean free path already at high temperature, in contrast with MAPbI₃ where it happens at 30 K. The overall temperature variation of κ in MASnI₃ seems to have a glassy behavior, which might stem from an effective scattering source spread over a larger temperature range. The ultralow thermal conductivity value of MASnI₃ is the key ingredient for high ZT . It is reasonable to assume the same value of κ for our MASnI₃ samples with different doping levels because a previous study showed that the Wiedemann–Franz electronic contribution to the thermal conductivity is negligible within this class of materials;⁶ however, for the more conductive samples of Takahashi et al.,¹⁰ an additional contribution of the charge carriers to the thermal conductivity (κ_{el}) cannot be neglected and has to be added.

The temperature dependency of ZT for MAPbI₃ (Figure 1d) and MASnI₃ (Figure 1h), calculated from the above-reported transport coefficients, increases globally with temperature. For MAPbI₃ in dark it reaches a maximum value of 10^{-9} only, just below room temperature. Photoinduced doping initiates an elevation of ZT because the electrical conductivity strongly increases, while S is maintained to a high value, yet ZT keeps very low, indicating that this form of doping is not sufficient for thermoelectric applications. Indeed, Hall-effect measurements yield a carrier density $n \approx 10^{14} \text{ cm}^{-3}$ and a carrier mobility $\mu \approx$

$13 \text{ cm}^2 \text{ V}^{-1} \text{ s}^{-1}$ for the strongest illumination condition, whereas theoretical calculations of He and Galli⁷ predict that $n \simeq 10^{18}$ to 10^{19} cm^{-3} is required to bring ZT close to unity. In the case of MASnI_3 , the most resistive sample has the magnitude well above the one of MAPbI_3 . Intentional (as reported in ref 10) or unintentional (as in our case) doping gives much higher conductivities, so that ZT at room temperature reaches the value of 0.13. This tendency is very promising, and it should be explored systematically in the future.

The evolution of ZT at room temperature is summarized in Figure 2 as a function of the electrical conductivity. It emphasizes that σ is the quantity which tunes ZT independently if its increase is due to the enhancement of the carrier density or of the charge mobility. We suppose that carrier mobility does not change substantially with doping, so this plot gives a good approximation for the variation of ZT with n , as well. As it can be seen in Figure 2, σ plays a dominant role in the modulation of ZT . Indeed, the difference in resistivity, two orders of magnitude between the nonilluminated and the illuminated MASnI_3 sample, does not result in a dramatic decrease in the thermoelectric power under the same condition.

For an efficient thermoelectric conversion and to compete with the best available materials, $ZT = 3$ is required. We speculate that increasing S , for example, by introducing some polaronic effects¹⁵ can be a rather complicated task and κ is already very low. Instead, doping $\text{CH}_3\text{NH}_3\text{SnI}_3$ will be the route to further increase ZT . According to the trend shown in Figure 2, one can extrapolate the room temperature resistivity necessary to satisfy this request: $\rho = 1 \times 10^{-3}$ to $3 \times 10^{-5} \Omega \text{ cm}$. This value is not more than two orders of magnitude lower than that observed in intentionally doped MASnI_3 crystals by Takahashi et al.^{10,12} In their work, they studied the effect of the dopant uptake during the crystal growth, under equilibrium conditions, from Sn^{II} and Sn^{IV} precursors. To quantitatively evaluate the carrier concentrations, they performed Hall effect measurements. They concluded that the dopant uptake was rather low; that is, the carrier concentration between the as-grown and the artificially doped MASnI_3 samples was increased by one order of magnitude only. However, this “ Sn^{II} and Sn^{IV} precursor”-doping can be instead regarded as self-doping. Hence this is not likely an effective way to shift the thermodynamic equilibrium between the Sn^{II} and Sn^{IV} ions in the resulted MASnI_3 crystal. Therefore, we suggest to shift and stabilize the Sn^{II} and Sn^{IV} redox equilibrium in the Sn-perovskite by doping with foreign cations having a stable oxidation state. For instance, the room-temperature conductivity of the single crystals of metallic slabs of the radical cation of ethylenedithio-1,2-diiodo-tetrathiafulvalene, EDT-TTF-I_2 , and polymeric lead iodide covalent anionic layers $(\beta\text{-(EDT-TTF-I}_2)_2^{\bullet+}[(\text{Pb}_{5/6}\square_{1/6}\text{I}_2)^{1/3-}]_3)$ has increased with two orders of magnitude upon doping with silver.¹⁶ Another path to achieve a higher electrical conductivity in the tin halide perovskite could be a postgrowth reduction of pristine or foreign cation-doped MASnI_3 .

IV. CONCLUSIONS

In the last couple of years hybrid halide perovskites have been in the focus of research for photovoltaic systems. $\text{CH}_3\text{NH}_3\text{PbI}_3$ has turned out to be a highly efficient material in converting solar light (photons) into electricity, even in fairly simple device configurations. Recently, interest has been drawn to the fact

that the same family of compounds might demonstrate good ability to convert heat into electricity. Thermoelectric devices, if their efficiencies stand high enough, could harvest waste heat and turn it into electricity or even be utilized in power plants. Thus, they would help to reduce the global consumption of nonrenewable energy. In our study, we measured the thermoelectric properties of $\text{CH}_3\text{NH}_3\text{PbI}_3$ and $\text{CH}_3\text{NH}_3\text{SnI}_3$. We show that ZT of the latter compound at room temperature can be enhanced by more than three orders of magnitude by chemical doping. Further engineering of this material could allow us to reach or even outclass the performance level of the presently most efficient thermoelectric devices. If, by a suitable doping, one could enhance the conductivity, ZT would increase toward unity and create a very performant material for such applications. In addition, $\text{CH}_3\text{NH}_3\text{SnI}_3$ was synthesized from a solution, potentially allowing for cheap and massive production, while it is considered as nontoxic. Biological assays for both compounds are still missing, though.

AUTHOR INFORMATION

Corresponding Author

*E-mail: xavier.mettan@epfl.ch.

Notes

The authors declare no competing financial interest.

ACKNOWLEDGMENTS

We thank Eric Bonvin for useful discussion. This work was supported by the Swiss National Science Foundation and partially by the CCEM funded HITTEC project.

REFERENCES

- (1) Snyder, G. J.; Toberer, E. S. Complex Thermoelectric Materials. *Nat. Mater.* **2008**, *7*, 105–114.
- (2) Bell, L. E. Cooling, Heating, Generating Power, and Recovering Waste Heat with Thermoelectric Systems. *Science* **2008**, *321*, 1457–1461.
- (3) Tritt, T. M.; Subramanian, M. A. Thermoelectric Materials, Phenomena, and Applications: A Bird's Eye View. *MRS Bull.* **2011**, *31*, 188–198.
- (4) Kraemer, D.; Poudel, B.; Feng, H.-P.; Caylor, J. C.; Yu, B.; Yan, X.; Ma, Y.; Wang, X.; Wang, D.; Muto, A.; et al. High-Performance Flat-Panel Solar Thermoelectric Generators with High Thermal Concentration. *Nat. Mater.* **2011**, *10*, 532–538.
- (5) Hsu, K. F.; Loo, S.; Guo, F.; Chen, W.; Dyck, J. S.; Uher, C.; Hogan, T.; Polychroniadis, E. K.; Kanatzidis, M. G. Cubic $\text{AgPb}_m\text{SbTe}_{2+m}$: Bulk Thermoelectric Materials with High Figure of Merit. *Science* **2004**, *303*, 818–821.
- (6) Pisoni, A.; Jaćimović, J.; Barišić, O. S.; Spina, M.; Gaál, R.; Forró, L.; Horváth, E. Ultra-Low Thermal Conductivity in Organic–Inorganic Hybrid Perovskite $\text{CH}_3\text{NH}_3\text{PbI}_3$. *J. Phys. Chem. Lett.* **2014**, *5*, 2488–2492.
- (7) He, Y.; Galli, G. Perovskites for Solar Thermoelectric Applications: A First Principle Study of $\text{CH}_3\text{NH}_3\text{AI}_3$ (A=Pb and Sn). *Chem. Mater.* **2014**, *26*, 5394–5400.
- (8) Horváth, E.; Spina, M.; Szekrényes, Z.; Kamarás, K.; Gaal, R.; Gachet, D.; Forró, L. Nanowires of Methylammonium Lead Iodide ($\text{CH}_3\text{NH}_3\text{PbI}_3$) Prepared by Low Temperature Solution-Mediated Crystallization. *Nano Lett.* **2014**, *14*, 6761–6766.
- (9) Jacimovic, J.; Mettan, X.; Pisoni, A.; Gaal, R.; Katrych, S.; Demko, L.; Akrap, A.; Forro, L.; Berger, H.; Bugnon, P.; et al. Enhanced Low-Temperature Thermoelectrical Properties of BiTeCl Grown by Topotactic Method. *Scr. Mater.* **2014**, *76*, 69–72.
- (10) Takahashi, Y.; Obara, R.; Lin, Z.-Z.; Takahashi, Y.; Naito, T.; Inabe, T.; Ishibashi, S.; Terakura, K. Charge-Transport in Tin-Iodide

Perovskite $\text{CH}_3\text{NH}_3\text{SnI}_3$: Origin of High Conductivity. *Dalton Trans.* **2011**, *40*, 5563–5568.

(11) Stoumpos, C. C.; Malliakas, C. D.; Kanatzidis, M. G. Semiconducting Tin and Lead Iodide Perovskites with Organic Cations: Phase Transitions, High Mobilities, and near-Infrared Photoluminescent Properties. *Inorg. Chem.* **2013**, *52*, 9019–9038.

(12) Takahashi, Y.; Hasegawa, H.; Takahashi, Y.; Inabe, T. Hall Mobility in Tin Iodide Perovskite $\text{CH}_3\text{NH}_3\text{SnI}_3$: Evidence for a Doped Semiconductor. *J. Solid State Chem.* **2013**, *205*, 39–43.

(13) Pantelides, S. The Electronic Structure of Impurities and Other Point Defects in Semiconductors. *Rev. Mod. Phys.* **1978**, *50*, 797–858.

(14) Hao, F.; Stoumpos, C. C.; Cao, D. H.; Chang, R. P. H.; Kanatzidis, M. G. Lead-Free Solid-State Organic–inorganic Halide Perovskite Solar Cells. *Nat. Photonics* **2014**, *8*, 489–494.

(15) Emin, D. Enhanced Seebeck Coefficient from Carrier-Induced Vibrational Softening. *Phys. Rev. B* **1999**, *59*, 6205–6210.

(16) Devic, T.; Evain, M.; Moëlo, Y.; Canadell, E.; Auban-Senzier, P.; Fourmigué, M.; Batail, P. Single Crystalline Commensurate Metallic Assemblages of π -Slabs and CdI_2 -Type Layers: Synthesis and Properties of β -(EDT-TTF- I_2) $_2$ [$\text{Pb}_{5/6}\square_{1/6}\text{I}_2$] $_3$ and β -(EDT-TTF- I_2) $_2$ [$\text{Pb}_{2/3+x}\text{Ag}_{1/3-2x}\square_x\text{I}_2$] $_3$, $X = 0.05$. *J. Am. Chem. Soc.* **2003**, *125*, 3295–3301.